

## ADVANCES IN STRAPDOWN SENSORS

By

AD-P003 620

Paul G. Savage  
 President  
 Strapdown Associates, Inc.  
 Woodbridge Plaza, Suite 150  
 10201 Wayzata Blvd.  
 Minnetonka, Minnesota 55343

## SUMMARY

This paper reviews the advances that have taken place in strapdown sensor technology since 1978. It is intended as an update to the paper on Strapdown Sensors presented as part of AGARD Lecture Series 95 in 1978 (1). Principal areas addressed in strapdown gyro technology are the state-of-the-art in mainstream floated rate-integrating and tuned-rotor strapdown gyros, performance advances in laser gyros, special design considerations associated with mechanically dithered laser gyros, the state-of-the-art in magnetic mirror and multioscillator laser gyros, present and projected application areas for laser gyros related to size, performance and cost, the theory of operation and state-of-the-art in fiber-optic rate sensor technology, and the fundamental distinctions between the laser gyro and fiber-optic rate sensor. Basic areas addressed in strapdown accelerometer technology are performance advances in pendulous accelerometers, and the theory of operation and state-of-the-art in vibrating beam accelerometer technology.

## 1. INTRODUCTION

The state-of-the-art in strapdown sensor technology has advanced considerably since 1978, particularly in the higher accuracy performance categories. Ring laser gyros designed by several manufacturing groups have demonstrated their ability to meet the requirements for 1 nmph inertial navigation. Laser gyros are now in operational use on several major aircraft programs, and have demonstrated reliabilities in the field that are exceeding user goals. Advanced development programs have been initiated to extend the performance capabilities of the ring laser gyro into the class needed for 0.1 nmph navigation.

Conventional floating rate-integrating and tuned-rotor gyro technology has been increasingly applied in the moderate to low performance strapdown areas. These instruments continue to provide a good alternative to the ring laser gyro in applications requiring small size and low cost, where lower performance is acceptable. A new optical rate sensor technology based on the use of fiber-optics has emerged over the past few years as a lower cost/reduced performance alternative to the ring laser gyro. Simultaneously, ring laser gyro development activities have been directed at cost and size reduction to extend its applicability range into the moderate performance areas.

Strapdown accelerometer technology continues to be principally based on the pendulous electrically servoed accelerometer design approach. Design refinements since 1978 have upgraded the performance of this instrument and somewhat reduced its cost. It continues to remain compatible in cost and performance with requirements in most strapdown application areas (in proportion to the cost of the gyro and computing elements that are also contained in a strapdown system). To meet cost targets for the future, a vibrating beam accelerometer technology is being developed as a lower cost alternative to the pendulous accelerometer.

This paper reviews each of the instruments discussed above, with emphasis on the performance capabilities, problem areas, and applications where they have been used or planned for use since 1978. For each instrument, a brief discussion is also included which describes its principal of operation. Analytical descriptions and detailed design considerations for the floated rate-integrating gyro, tuned-rotor gyro, ring laser gyro, and pendulous accelerometer have been provided in the AGARD Lecture Series 95 paper on Strapdown Sensors (1), and are not repeated here. Error characteristics for the fiber-optic rate sensor and vibrating beam accelerometer are presented, but from a qualitative standpoint, because the performance characteristics of these devices have not been sufficiently disclosed in the open literature to allow detailed accurate analytical modeling that accounts for the important critical error sources, particularly those that are environmentally induced and which change over time and operating cycles.

A generalized error budget is also provided for reference at the beginning of the paper which attempts to define typical gyro and accelerometer performance requirements for four types of strapdown inertial systems.

## 2. SENSOR PERFORMANCE REQUIREMENTS

areas: the classical 1 nmph inertial navigator, a higher performance advanced 0.1 nmph inertial navigator, a lower performance strapdown attitude heading reference system (AHRS), and a still lower performance tactical missile midcourse guidance system. The performance categories depicted in Table 1 are considered typical for most strapdown sensor applications today and in the immediate future. Table 1 should be used as a reference to categorize typical sensor performance requirements during discussions on individual sensor capabilities.

TABLE 1 - TYPICAL STRAPDOWN SENSOR PERFORMANCE REQUIREMENTS

Performance Parameter	0.1 nmph INS	1.0 nmph INS	AHRS	Tactical Missile Midcourse Guidance
Gyro Bias Uncertainty (deg/hr)	0.001	0.01	1.0(0.1)* to 10	5 to 30
Gyro Random Noise (deg/hr <sup>1/2</sup> )**	0.005	0.002	0.01	0.1
Gyro Scale-Factor Uncertainty (ppm)	1	5	200	1000
Gyro Alignment Uncertainty (arc sec)	1	2	200	300
Accelerometer Bias Uncertainty ( $\mu$ g)	10	40	1000	1000
Accelerometer Scale-Factor Uncertainty (ppm)	50	200	1000	1000
Accelerometer Alignment Uncertainty(sec)	3	7	200	300
Accelerometer Bias Trending ( $\mu$ g/sec)	0.003	0.01	NA(0.1)*	NA

\* For AHRS with an earth rate gyro-compass heading determination requirement. Other figure shown is for AHRS with heading slaved to magnetic flux heading detector.

\*\* This error source is a characteristic principally of laser gyros.

### 3. SINGLE-DEGREE-OF-FREEDOM FLOATED RATE-INTEGRATING GYRO

The floated rate-integrating gyro (1, 4, 5) pictured schematically in Figure 1 is the gyro with the longest production history and is the original high-accuracy gimbale-platform gyro. The device consists of a cylindrical hermetically sealed momentum-wheel/spinmotor assembly (float) contained in a cylindrical hermetically sealed case. The float is interfaced to the case by a precision suspension assembly that is laterally rigid (normal to the cylinder axis) but allows "frictionless" angular movement of the float relative to the case about the cylinder axis. The cavity between the case and float is filled with a fluid that serves the dual purpose of suspending the float at neutral buoyancy, and providing viscous damping to resist relative float-case angular motion about the suspension axis.

A ball-bearing or gas-bearing synchronous-hysteresis spinmotor is utilized in the float to maintain constant rotor speed, hence constant float angular momentum. A signal-generator/pickoff provides an electrical output signal from the gyro proportional to the angular displacement of the float relative to the case. An electrical torque generator provides the capability for applying known torques to the float about the suspension axis proportional to an applied electrical input current. Delicate flex leads are used to transmit electrical signals and power between the case and float.

Under applied angular rates about the input axis, the gyro float develops a precessional rate about the output axis (rotation rate of the angle sensed by the signal-generator/pickoff, see Figure 1). The pickoff-angle rate generates a viscous torque on the float about the output axis (due to the damping fluid) which sums with the electrically applied torque-generator torque to precess the float about the input axis at the gyro input rate. The pickoff-angle rate thereby becomes proportional to the difference between the input rate and the torque-generator precessional rate, hence, the pickoff angle becomes proportional to the integral of the difference between the input and torque-generator rates.

To operate the gyro in a strapdown mode, the pickoff angle is electrically servoed to null by the torque generator which is driven by the signal-generator/pickoff output (through suitable compensation and amplifier electronics). The time integral of the difference between the input and torque-generator precessional rates is thereby maintained at zero, and the integral of the torque-generator rate becomes proportional to the integral of the input rate. Thus, the integral of the torque-generator electrical current provides a measure of the integral of input rate for a rate-gyro strapdown inertial navigation system.

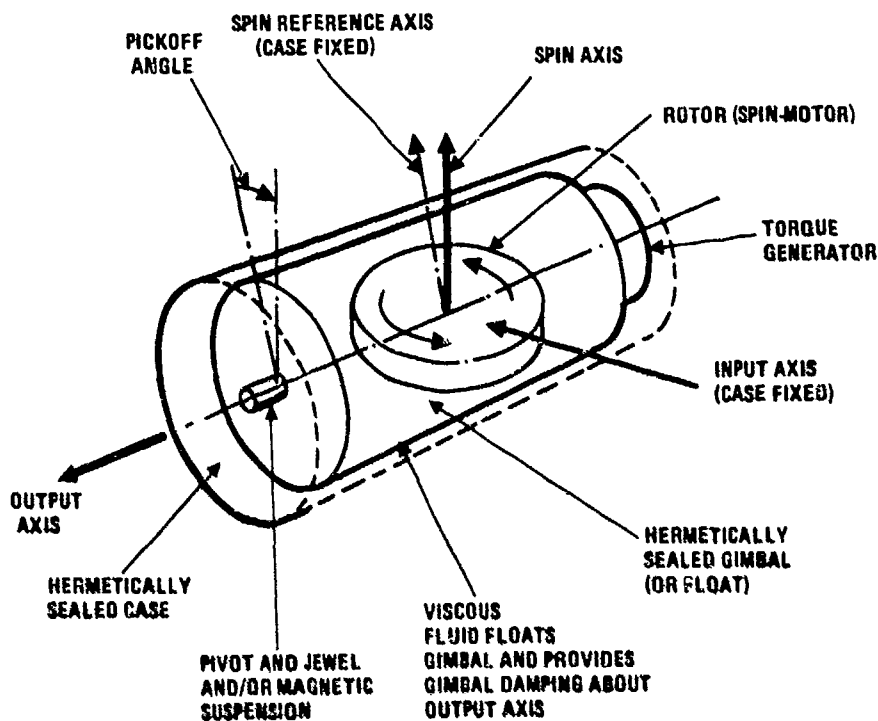


Figure 1 - Single-degree-of-freedom floated rate-integrated gyro concept.

### 3.1 Performance And Application Areas

Application areas for the strapdown floated rate-integrating gyro (RIG) have been primarily in the lower performance (5 to 30 deg/hr bias accuracy) areas where small-size low angular momentum units meet performance requirements, and costs are competitive with alternative gyro mechanization approaches (e.g., the tuned-rotor gyro). The floatation fluid suspension in the RIG makes the device extremely rugged, hence, provides a natural suitability to those lower performance application areas where high vibrations and shock are prevalent.

Low cost tactical missile midcourse inertial guidance has been a continuing application area for the strapdown RIG. Standard Missile-2, Harpoon, Phoenix, and recently SMRAAM, are examples of tactical missile systems that incorporate strapdown RIG's for midcourse guidance and stabilization/control. Strapdown RIG's have also been used in some applications to implement a short term navigation reference between updates from a higher accuracy navigation device. Examples are motion compensation for airborne radar systems (using the aircraft INS as the "outer-loop" reference), and to generate short term navigation data between precision radio navigation position fixes for aircraft test instrumentation purposes (e.g., ACMR - Air Combat Maneuvering Range).

Higher performance application areas for the strapdown RIG have remained limited due to their higher cost for comparable performance compared to the strapdown tuned-rotor or ring laser gyros.

### 4. TUNED-ROTOR GYRO

The tuned-rotor gyro (1, 6, 7, 8, 9, 10) is the most advanced gyro in large-scale production today for aircraft 1-nmi/hr gimballed platforms. Due to its simplicity (compared to the floated rate-integrating gyro), the tuned-rotor gyro is theoretically lower in cost

and more reliable. A drawing of a representative tuned-rotor gyro is presented in Figure 2. Figure 3 is a schematic illustration of the gyro rotor assembly.

The gyro consists of a momentum wheel (rotor) connected by a flexible gimbal to a case-fixed synchronous-hysteresis ball-bearing spinmotor drive shaft. The gimbal is attached to the motor and rotor through members that are torsionally flexible but laterally rigid. A two-axis variable-reluctance signal-generator/pickoff is included that measures the angular deviation of the rotor (in two axes) relative to the case (to which the motor is attached). Also included is a two-axis permanent-magnet torque generator that allows the rotor to be torqued relative to the case on current command. The torquer magnets are attached to the rotor, and the torquer coils are attached to the gyro case.

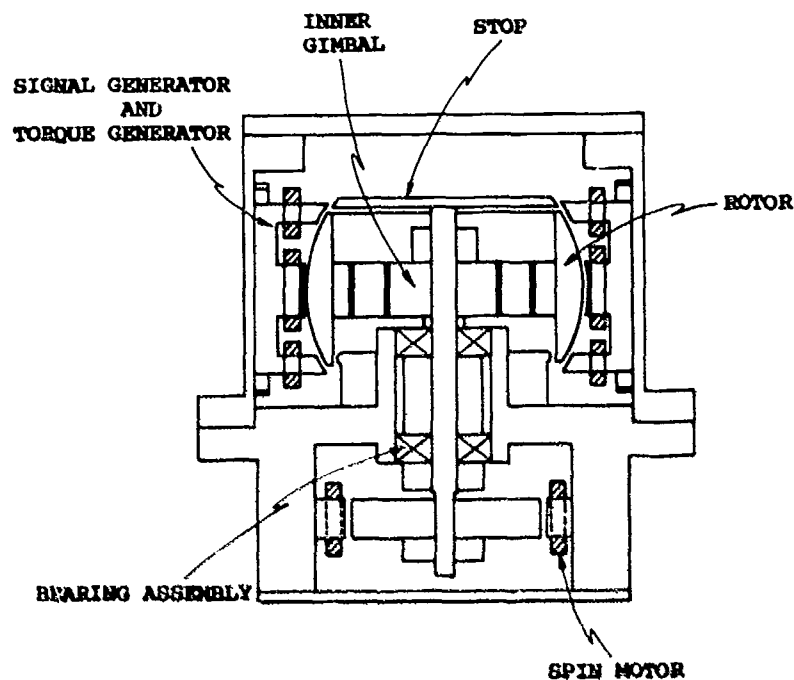


Figure 2 - Typical tuned-rotor gyro configuration.

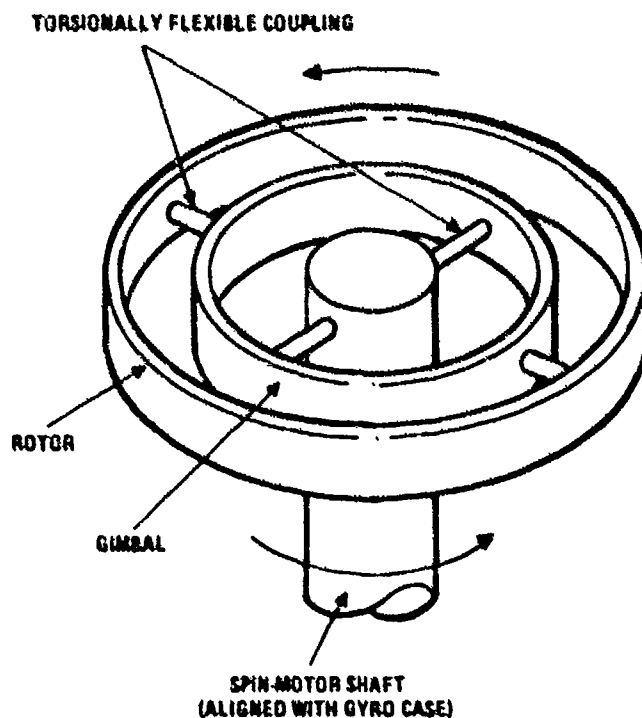


Figure 3 - Tuned-rotor gyro rotor assembly.

As for all angular-momentum-based rate-sensing devices, the key design feature of the gyro is the means by which it can contain the reference momentum (the spinning rotor), without introducing torques (drift rates) in the process. For the tuned-rotor gyro, the method is linked to the dynamic effect of the flexible gimbal attachment between the rotor and the motor. Geometrical reasoning reveals that when the rotor is spinning about an axis that deviates in angle from the motor-shaft axis, the gimbal is driven into a cyclic oscillation in and out of the rotor plane at twice the rotor frequency. Dynamic analysis shows that the reaction torque on the rotor to sustain this motion has a systematic component along the angular-deviation vector that is proportional to the angular displacement, but that acts as a spring with a negative spring constant. The flexible pivots between the rotor and gimbal, on the other hand, provide a similar spring torque to the rotor, but of the opposite sign. Hence, to free the rotor from systematic torques associated with the angular displacement, it is only necessary to design the gimbal pivot springs such that their effect cancels the inverse spring effect of the gimbal. The result (tuning) is a rotor suspension that is insensitive to angular movement of the case.

Use of the tuned-rotor gyro in a strapdown mode parallels the technique used for the floated rate-integrating gyro. Exceptions are that damping must be provided electrically in the caging loop, as there is no fluid, and that the gyro must be caged in two axes simultaneously. The latter effect couples the two caging loops together due to the gyroscopic cross-axis reaction of the rotor to applied torques.

#### 4.1 Performance And Application Areas

Application areas for the strapdown tuned-rotor gyro (TRG) have been primarily in the medium performance areas where small-size low angular momentum units have acceptable accuracy, are lower in cost compared with comparable size/performance ring laser gyro technology, and where bias accuracy compared to equivalent cost RIG units is superior. The inherent simplicity in design of the dry rotor suspension concept for the TRG which lowers its production cost, also limits its usefulness in high vibration/shock environments where rotor resonances can potentially be excited (producing sensor error and, in extreme cases, device failure). Current design improvements for the TRG are being directed at extending its vibration capability while retaining accuracy.

The strapdown AHRS (attitude-heading reference system) has been a primary application area for the strapdown TRG for commercial aircraft, military drones, and most recently, torpedoes. One of the larger potential application areas for the strapdown TRG is for the military aircraft strapdown AHRS where small size and low cost are key requirements, and not yet achievable with ring laser gyro technology.

Two current application areas of interest for the strapdown TRG are for tactical missile midcourse guidance and helicopter or torpedo strapdown AHRS. Small-size low-cost versions of the strapdown TRG have been developed as a competitor to the RIG for the tactical missile midcourse guidance application. Potential vibration/shock susceptibility of the TRG is an area of concern for the tactical missile application, but is being addressed by TRG design groups. Shock requirements for torpedo application of the TRG have been handled through use of elastomeric isolators between the TRG sensor assembly and torpedo mounting plate. The helicopter AHRS application imposes a bias stability requirement of 0.1 deg/hr on the TRG which is not achievable today with small size low cost units.

The 0.1 deg per hour helicopter AHRS requirement stems from the need to determine heading prior to takeoff by earth-rate gyro-compassing to an accuracy of 0.5 degrees. This translates into a gyro accuracy requirement of 0.1 deg/hr to detect the direction of horizontal earth rate (at 45 deg latitude) to 0.01 radians (i.e., 0.5 degrees). Typical small-size low-cost TRG's have bias accuracies over long term of 1 to 2 deg/hr. To achieve the 0.1 deg/hr requirement, a turn-table is needed to position the TRG at different orientations relative to the earth rate vector during initial alignment operations. In this way, repeatable gyro biases can be measured and separated from earth rate measurements, and earth rate measurements to the required 0.1 deg per hour accuracy become achievable. The turn-table also provides the means for calibrating the heading gyro scale factor prior to takeoff. The use of such a turn-table as an integral part of a strapdown TRG system for the helicopter AHRS is considered standard practice today.

##### 4.1.1 Design Considerations In A Dynamic Environment

Use of a strapdown TRG (or RIG) in a dynamic vibration environment must address the basic question of wide versus narrow bandwidth for the torque-rebalance loop. If a significant angular vibration environment exists, the loop bandwidth must be broad enough to measure real angular rates that integrate into attitude/heading (33, 34). On the other hand, if the bandwidth is too broad, undesirable high frequency sensor error effects will be amplified and passed as output data to the attitude integration process, generating attitude error. In the case of the tuned-rotor gyro, undamped rotor wobble effects near spin frequency limit the maximum bandwidth that is practically achievable to approximately 80Hz. The minimum torque-rebalance bandwidth is selected so that the gyro rate signal outputs, when integrated, generate attitude data that:

1. Accurately accounts for the accelerometer attitude under combined angular/linear vibration environments (i.e. - sculling (33, 34)).
2. Accurately accounts for multiaxis angular vibration rates that rectify into attitude drift (i.e., coning (33, 34)).

In the case of the TRG, Item 2 is achievable with lower bandwidth than with the RIG because of the inherent nature of the TRG being an attitude sensing instrument (i.e., the pickoff signals measure the true attitude orientation of the gyro case relative to the rotor). As such, attitude errors in the TRG generated by low bandwidth limits, are theoretically recoverable (with a time delay) by proper torque-loop rebalance logic. This contrasts with the RIG torque-loop because the pickoff signal in the RIG represents the integrated input rate (not attitude). As such, the RIG bandwidth must be broad enough to accurately measure all significant multiaxis angular vibrations so that the true attitude can be properly constructed in the attitude integration process. Both the RIG and TRG bandwidths have comparable requirements to satisfy Item 1.

One of the principal error mechanisms for torque-rebalance gyros under dynamic environments is torquer heating effects. In addition to producing scale factor errors in the gyro output, bias errors can be produced by associated thermal gradient effects across the instrument. In the case of the gyro scale factor error, much of the temperature induced effect can be eliminated by temperature measurement and modeling correction in the strapdown computer. Unfortunately, for the tuned-rotor gyro, because the torquer magnet is attached to the spinning rotor, direct temperature measurements are difficult to achieve due to the problem of making electrical measurements across the spinning rotor bearings (without resorting to slip-rings and attendant potential reliability problems).

In order to reduce the scale factor error variation with temperature, TRG manufacturers have developed new magnet materials (e.g., doped samarium cobalt) which has a lower scale factor error as a function of temperature. The penalty is reduced magnet strength, hence, a larger magnet to generate the same torque capability. Note, that the torquer heating effect under angular vibration can also be reduced by lowering the bandwidth of the torque-rebalance loop. In the case of the TRG, this technique has been used in helicopter applications as a compromise between sensor error amplification versus output signal attenuation error. Because the TRG is more tolerant of low bandwidth operation (see previous discussion on Item 2 requirements), a reasonable compromise can usually be found. However, the bandwidth selection then becomes sensitive to vehicle installation and operating condition. In general, no true optimum solution is possible.

Scale factor errors in strapdown gyros under maneuvering flight conditions can rectify into attitude drift in the strapdown system computer (2, 34). The classical effect is through continuous turning in one direction that generates a net attitude error proportional to the product of the scale factor error with the net angle traversed. Cyclic maneuvers can also produce net attitude error buildup; asymmetrical scale factor errors rectify under oscillatory rates about the gyro input axis, symmetrical scale factor errors rectify under multiaxis rates that are phased ninety degrees apart (between axes). The classical case of the latter effect is the "jinking maneuver" which consists of cyclic patterns of roll right, turn right, roll left, turn left. In the case of the tuned-rotor gyro, the scale factor error effect must be assessed to assure compliance to accuracy requirements for the particular application being considered. Reduction of the gyro torquer scale factor temperature coefficient in future versions should broaden the areas of applicability for the instrument in a dynamic environment.

## 5. RING LASER GYRO

Unlike the gyros that utilize rotating mass for angular measurement reference, the laser gyro operating principal is based on the relativistic properties of light (1, 11, 12, 14). The device has no moving parts; hence, it has the potential for extremely high reliability.

Figure 4 depicts the basic operating elements in a laser gyro: a closed optical cavity containing two beams of correlated (single-frequency) light. The beams travel continuously between the reflecting surface of the cavity in a closed optical-path; one beam travels in the clockwise direction, the other in the counterclockwise direction, each occupying the same physical space in the cavity. The light beams are generated from the lasing action of a helium-neon gas discharge within the optical cavity. The reflecting surfaces are dielectric mirrors designed to selectively reflect the frequency associated with the helium-neon transition being used.

To understand the operation of the laser gyro, consider the effect of cavity rotation on an observer rotating with the cavity. Relative to the observer, it takes longer for a photon of light to traverse the distance around the optical path in the direction of rotation than in the direction opposite to the rotation. This effect is interpreted by the observer as a lengthening of the net optical path length in the direction of rotation, and a shortening of the path length in the opposite direction. Because the laser beam is self-resonating, it is a continuous beam that propagates around the cavity, closing on itself without discontinuity. As a result, the effect of the self-resonance is to maintain a fixed integral number of light wave lengths around the cavity. Under input angular rate, the increase in optical path length experienced by the beam traveling in the direction of rotation, must therefore

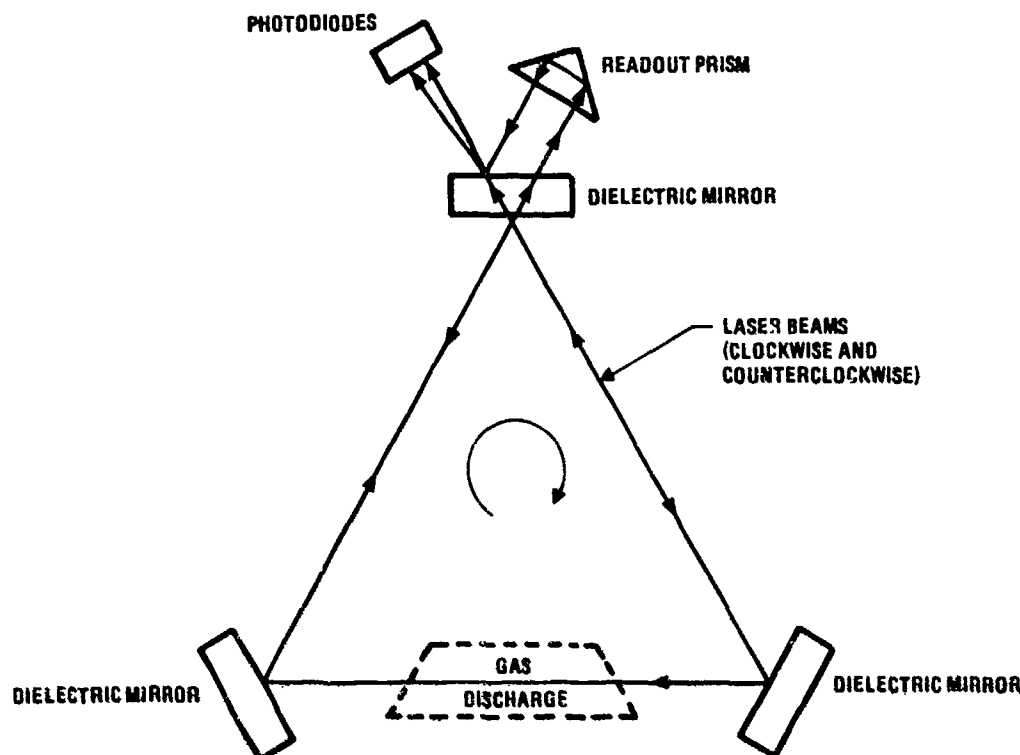


Figure 4 - Laser gyro operating elements.

be accompanied by a proportional increase in wavelength to maintain the same integral number of waves around the lengthened cavity. The converse is true for the beam traveling opposite to the direction of rotation. Thus, a wavelength difference is established between the oppositely directed beams proportional to the optical path length change, hence, proportional to the input angular rate. Because the speed of light is constant, the wavelength difference is accompanied by a frequency difference between the two beams in the opposite sense. Hence, a frequency difference is generated between the two beams that is proportional to input rotation rate.

The frequency difference is measured in the laser gyro by allowing a small percentage of the laser radiation to escape through one of the mirrors (Figure 4). An optical prism is typically used to reflect one of the beams such that it crosses the other in almost the same direction at a small angle (wedge angle). Due to the finite width of the beams, the effect of the wedge angle is to generate an optical fringe pattern in the readout zone. When the frequencies between the two laser beams are equal (under zero angular rate input conditions), the fringes are stationary relative to the observer. When the frequencies of the two beams are different (under rotational rates), the fringe pattern moves relative to the observer at a rate and direction proportional to the frequency difference (i.e., proportional to the angular rate). More importantly, the passage of each fringe indicates that the integrated frequency difference (integrated input rate) has changed by a specified increment. Hence, each fringe passage is a direct indication of an incremental integrated rate movement, the exact form of the output needed for a rate-gyro strapdown navigation system.

Digital integrated-rate-increment pulses are generated from the laser gyro from the outputs of two photodiodes mounted in the fringe area and spaced 90 degrees apart (in fringe space). As the fringes pass by the diodes, sinusoidal output signals are generated, with each cycle of a sine wave corresponding to the movement of one fringe over the diodes. By observing which diode output is leading the other (by 90 degrees), the direction of rotation is determined. Simple digital-pulse triggering and direction logic operating on the photodiode outputs convert the sinusoidal signal to digital pulses for computer input.

The analytical relationship between the fringe angle change and integrated rate input angle change (11, 12, 34) is given by:

$$\Delta\theta = \frac{B \pi A}{\lambda L} \Delta\theta \quad (1)$$

where

- $\Delta\phi$  = Gyro fringe angle output change (Note:  $\Delta\phi = 2\pi$  for a movement of one fringe across the output photodiode).
- A = Area enclosed by the laser beam.
- L = Perimeter of the laser beam path.
- $\lambda$  = Laser wavelength (e.g., 0.63 micron).
- $\Delta\theta$  = Integrated input rate into the gyro (Note:  $\Delta\theta = 2\pi$  for a complete 360 degree input rotation angle).

The "pulse size" for the laser gyro is the value of  $\Delta\theta$  for which  $\Delta\theta = 2\pi$  (i.e., the input angle which produces a full fringe movement of  $2\pi$  across the photodiode output detector). It is easily verified that for an equilateral triangle laser gyro with 12.6 inch perimeter (4.2 inches per side), the pulse size for a 0.63 micron laser (typical of today's technology) is 2 arc seconds.

The digital pulse output logic can be mechanized to output a pulse each time a full fringe has passed across the diode (e.g., by triggering on the positive going zero crossing from one of the readout photodiodes). For this approach, the gyro output pulse scaling would equal the "pulse-size" defined above. Alternatively, gyro output pulses can be triggered at the positive and negative-going zero crossings from each of the two photodiodes to achieve an output pulse scaling that is four times finer than the basic full-fringe "pulse-size". Both of the latter approaches are used today.

### 5.1 Construction

Figure 5 illustrates a typical laser gyro mechanization concept. A single piece structure (typically Zerodur, a ceramic glass material) is used to contain the helium-neon gas, with the lasing mirrors and electrodes forming the seals. High voltage (typically 1500 volts) applied across the electrodes (one cathode and two anodes) maintains the helium-neon gas mixture in an ionized state, thereby providing the required laser pumping action. High-quality optical seals are used to avoid introducing contaminants into the helium-neon mixture, which would degrade performance and ultimately limit life-time.

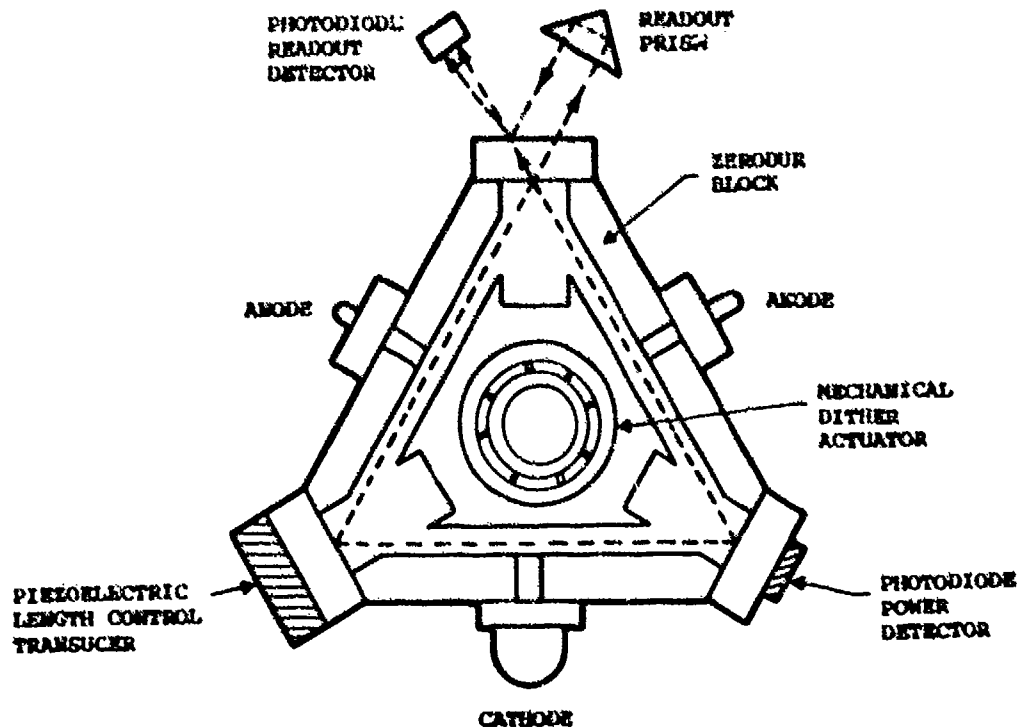


Figure 5 - Laser-gyro block assembly.

The accuracy of the laser gyro depends on the manner in which the laser beams are affected by the influences of the lasing cavity. A key requirement in this regard is that the average of the clockwise and counterclockwise path lengths around the lasing triangle be constant. Many of the error characteristics in the laser gyro vary as a function of average path length (12), hence, stabilizing average path length also implicitly stabilizes performance. Zerodur is used to construct the laser gyro optical cavity due to its low coefficient of thermal expansion, hence, high degree of path-length stability.

To compensate for residual remaining path-length variations, a piezoelectric transducer is mounted on one of the laser gyro mirror substrates (see Figure 5). Actuation of the transducer by a control voltage flexes the mirror substrate to effect a path-length change. The control signal for the transducer is designed to maintain peak average power in the lasing beams. Because average beam power varies cyclically with path-length multiples of laser wavelength, maintaining peak lasing power implicitly controls the average path-length to a constant value. The average beam power is detected in the laser gyro by a photodiode mounted on one of the mirrors that senses a small percentage of the combined radiation from the clockwise and counterclockwise beams.

### 5.1.1 Square Versus Triangular Ring Laser Gyros

Figure 6 illustrates a square laser gyro geometry utilizing four mirrors (as contrasted with the three-mirror triangular configuration in Figure 5). Both geometries are used today by competing ring laser gyro manufacturers. The rationale espoused by proponents of the triangular versus square geometry can be summarized as follows: Proponents of the triangular geometry point to the three-mirror configuration as having the minimum mirror count to form an enclosed laser ring. As a result mirror costs per gyro are minimized, and lock-in (a performance deficiency in the laser gyro to be discussed in the next section) is reduced due to the minimum number of scatterers (the mirrors) in the laser beam path. From a manufacturing standpoint, the proponents of the triangle point out that alignment of the mirrors on the gyro block is simplified (hence, cost reduced) because the triangle geometry is self-aligning in the lasing plane (through use of one curved mirror), and alignment out of the lasing plane is readily achieved by out-of-plane adjustment of the curved mirror during device assembly.

Proponents of the square laser gyro geometry consider the additional mirror cost a negligible penalty when technology advances are taken into account. The additional alignment requirement for the fourth mirror in a square is identified as a benefit by square gyro proponents due to the added flexibility it affords to adjust beam/cavity positioning, and thereby optimize performance. Another performance advantage identified for the square

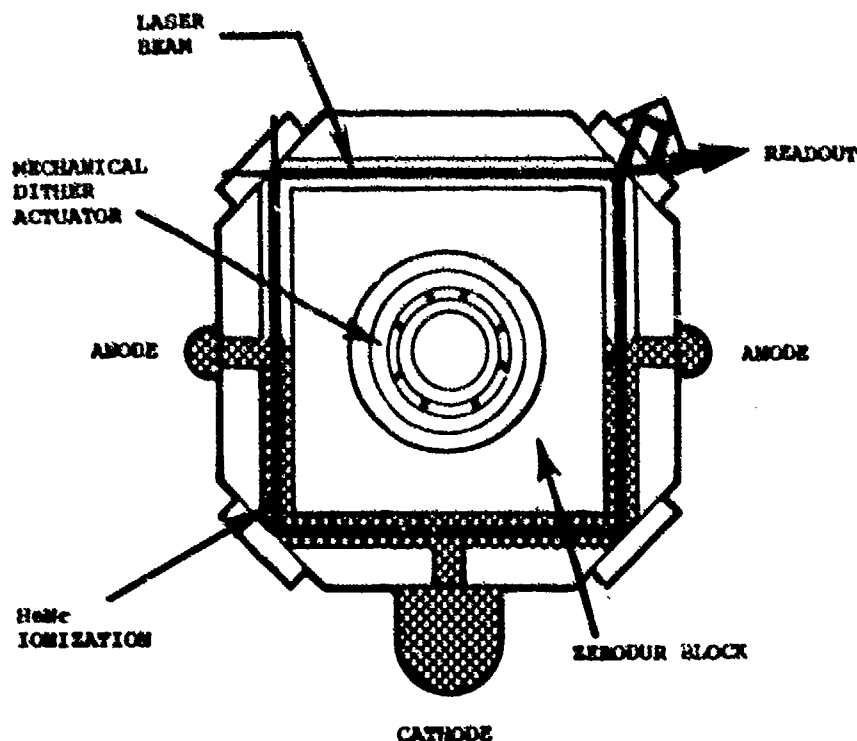


Figure 6 - Square laser gyro configuration.

is its higher area-to-perimeter ratio compared to a triangle of the same size, which directly increases accuracy. The area-to-perimeter ratio (see Equation (1)) is the primary parameter in the device that impacts performance (12, 13, 17). Proponents of the square also point to the lower angle of incidence at the laser beam/mirror interface which reduces back-scattering per mirror. The net result is a combined mirror reduction in back-scattering which more than compensates for the additional mirror scattering, hence, reduces overall gyro lock-in. Finally, from a manufacturing standpoint, square laser gyro enthusiasts claim simpler tooling and machining for square compared to triangular devices, hence, reduced production costs.

Triangular laser gyro proponents acknowledge a performance penalty due to the less favorable area-to-perimeter ratio and beam-incidence geometry. However, they claim that this advantage is minor and will be largely overcome by technology advances. Additionally, triangle proponents argue that when the gyro electrodes (size and geometry) are taken into account, no real size advantage exists for the square gyro configuration. From a machining standpoint, triangle proponents claim no advantage exists for any particular geometry once tooling is complete and experience has been attained.

At this stage in the laser gyro development cycle, it is not clear whether one geometry is superior to another as a general rule.

## 5.2 Lock-In

The phenomenon of lock-in continues to be the most prominent error source in the laser gyro and the most difficult to handle. The means for compensating lock-in has been the principal factor determining the configuration and performance of laser gyros from different manufacturers.

The phenomenon of laser gyro lock-in arises because of imperfections in the lasing cavity, principally the mirrors, that produce back-scattering from one laser beam into the other (13). The resulting coupling action tends to pull the frequencies of the two beams together at low rates producing a scale-factor error. For slowly changing rates below a threshold known as the lock-in rate, the two beams lock together at the same frequency producing no output (i.e., a dead zone). Figure 7 illustrates the effect of lock-in on the output of the laser gyro as a function of input rate for slowly changing input rate conditions. The magnitude of the lock-in effect depends primarily on the quality of the mirrors. In general, lock-in rates on the order of 0.01 to 0.1 degree-per-second are the lowest levels achievable with today's laser gyro technology (with 0.63-micron laser wavelength). Compared with 0.01 deg/hr navigation requirements, this is a serious error source that must be overcome.

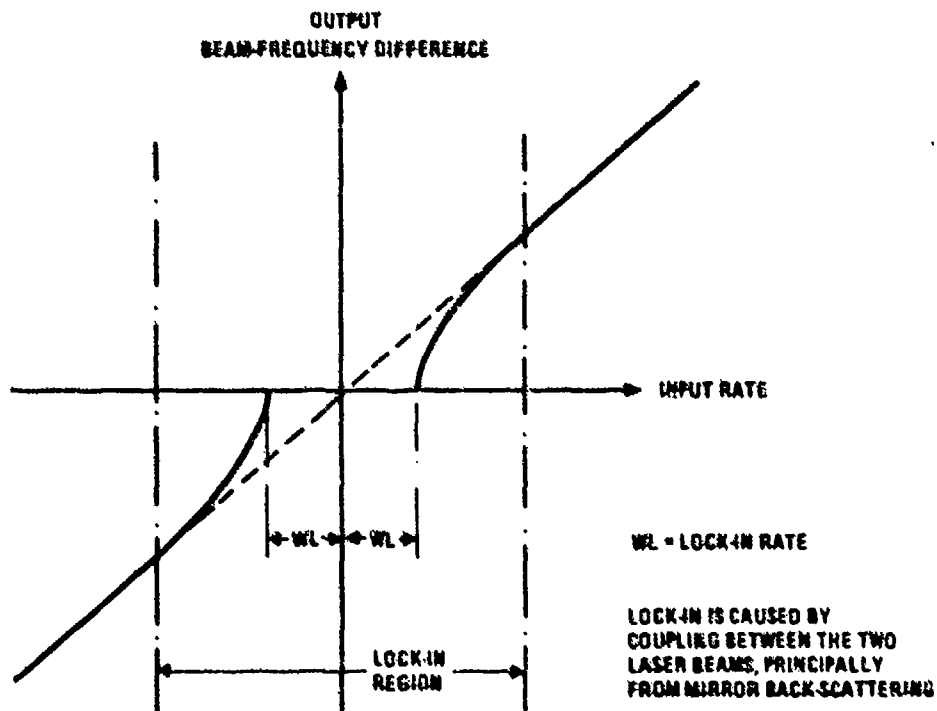


Figure 7 - Laser gyro lock-in.

Under dynamic input rates that rapidly pass through the lock-in region, the effect of lock-in is to introduce a small angle error in the gyro output as the lock-in zone is traversed, but still retaining sensitivity to input rate while in the lock-in region (i.e., no hard dead-zone develops as in Figure 7 (12, 13, 16). The latter effect underlies the basic principal behind adding cyclic high rate bias to the laser gyro as a means for circumventing the lock-in dead-zone effect, and converting it into a random angle error added to the gyro output each time the biased gyro input cycles through the lock-in region. The principal method being used today to generate the oscillating bias in the laser gyro is mechanical dither.

### 5.2.1 Mechanical Dither

With mechanical dither, the oscillating bias into the laser gyro is achieved by mechanically vibrating the gyro block at high frequency about its input axis through a stiff dither flexure suspension built into the gyro assembly. The spoked-like structures in Figures 5 and 6 conceptually illustrate such a flexure that is attached to the laser block (on the outside) and to the gyro case/mount (on the inside) by metal rings that are connected to each other by flexible metal reeds. Piezoelectric transducers attached to the reeds provide the dither drive mechanism to vibrate the gyro block at its resonant frequency about the input axis. One piezoelectric transducer is mechanized as a dither angle readout detector and used as the control signal to generate voltage into the drive piezo's to sustain a specified dither amplitude. The dither angle amplitude and acceleration are designed so that the dwell time in the lock-in zone is short so that hard lock-in will never develop. The result is a gyro that has continuous resolution over the complete input rate range. The residual effect of lock-in is a small random angle error in the gyro output that is introduced each time the gyro passes through lock-in (at twice the dither frequency). This is the principal source of random noise in mechanically dithered laser gyros. The relationship between laser gyro random noise, lock-in, and dither rate is ideally given by (15):

$$\sigma_R = \frac{Q_L}{(Q_D K)^2} \quad (2)$$

where

$\sigma_R$  = Gyro random noise (or "random walk") coefficient (deg/hr<sup>1/2</sup>)

$Q_L$  = Lock-in rate

$Q_D$  = Dither rate amplitude

$K$  = Gyro output scale factor in fringes per input revolution (i.e., the reciprocal of the gyro "pulse size" discussed previously, times  $2\pi$ )

For typical values of  $\sigma_R = 0.002$  deg/hr<sup>1/2</sup>,  $Q_L = 0.01$  deg/sec, and  $K = 648,000$  (i.e., 2 arc sec pulse size), equation (2) can be used to show that  $Q_D = 72$  deg/sec. To achieve sufficient lateral stiffness, the dither spring is designed such that the frequency of the dither motion is on the order of 400 Hz. The associated dither cycle amplitude (corresponding to 72 deg/sec dither rate) is 103 arc sec (or 206 arc sec peak-to-peak). Equation (2) is based on the assumption that the angle error generated in the gyro output is uncorrelated from dither cycle to cycle. In practice, this is not perfectly achievable, and somewhat larger dither amplitudes are required than predicted by equation (2). Nevertheless, the figures presented previously are generally representative of typical mechanical dither requirements.

Once mechanical dither is incorporated for lock-in compensation, means must be provided to remove the oscillating bias signal from the gyro output (so that the gyro output represents the motion of the sensor assembly to which the gyro is mounted). Figure 5 illustrates the "case mounted readout" method of optically cancelling the dither from the output. By mounting the readout reflecting prism and photodiodes on the gyro case (i.e., off the gyro block) the translational movement of the gyro block relative to the case (caused by dither) will generate fringe motion at the photodiodes. This purely geometrical effect can be made to cancel the fringe movement produced by the laser block sensed dither angular motion through proper selection of the rotational center for the mechanical dither mount. The result is a photodiode output signal that responds to rotation of the gyro case and not relative movement between the dithering gyro relative to the case.

The alternative to "case-mounted readout" is "block-mounted readout" as illustrated in Figure 6. With this approach the gyro readout optics are mounted directly to the gyro block. Relative movement between the block and case is removed by measurement and subtraction, or by filtering. In the measurement/subtraction approach, a transducer (typically electromagnetic) is used to electrically measure the instantaneous angle between the gyro block and case. The electrical signal is then digitized and subtracted from the gyro pulse output for dither motion compensation. With the filter approach, a digital filter is used to filter signals near and above the dither frequency from the gyro output.

The result is a cancellation of the unwanted dither rate between the gyro block and case. The penalty is attenuation of real oscillating rates of the gyro case which, if significant, must be accurately measured for processing in the strapdown computer. Use of the filter approach is only valid for relatively benign environment applications where it can be assured that the only angular rate signals that need to be measured have frequency content well below the dither frequency.

**5.2.1.1 Mechanical Dither Design Complications** - Originally touted as a simple solution to the lock-in problem with no deleterious side effects, the mechanical dither concept applied in practice has been found to be the source of several subtle mechanical coupling error mechanisms that must be designed for at the three-gyro system level for solution (19, 34). It must be realized at the onset, however, that these complications are directly proportional to the magnitude of dither motion required for lock-in compensation. As lock-in rates are reduced, dither amplitudes can be reduced proportionally (see equation (2)), and design solutions for the effects described below can be more easily achieved.

The basic problem with mechanical dither stems from a kinematic property of three-axis rotary motion that cyclic rates in two orthogonal axes, if at the same frequency but phase shifted by ninety degrees, will produce a real constant attitude rate about the third axis (33, 34). The effect, known as "coning", if present, must be measured as cyclic rate signals by the strapdown gyros, and delivered to the strapdown computer so that the true drift about the third axis will be properly calculated. The problem arises when gyro output errors are also being generated at the same frequency as the real rates to be measured. Cyclic error signals from the gyro in one axis, in combination with errors or real cyclic rates from the gyro in one of the other orthogonal axes, will produce a vector rate profile which appears as coning, but is false ("pseudo-coning" is the nonmenclature typically used to describe this phenomenon). Since the composite gyro output signals (real plus error) are processed in the same computer used to measure real coning motion, a pseudo-coning error will be created in the strapdown computer as a false drift rate about the "third" axis. Filtering the gyro signals to remove the output error oscillations is not acceptable if real cyclic motion is present, since the true drift caused by the real cyclic coning motion will not be properly measured and accounted for.

In the case of mechanically dithered laser gyros, a potential source of real high frequency coning in a strapdown system is the reaction torque of the gyro dither drives into the sensor assembly (the sensor assembly typically consists of a metal casting to which the gyros and accelerometers are mounted). To minimize dither reaction torque resonance effects, and to provide compliance for thermal expansion, most RLG sensor assemblies are mechanically isolated from the system chassis by elastomeric isolators (34). To generate coning motion, equal angular rate vibration frequencies must exist simultaneously in two orthogonal axes. Dither induced vibrations from nominally orthogonal laser gyros into the sensor assembly can become frequency correlated between axes if mechanical coupling exists between the axes (e.g., principal moment-of-inertia axes of the sensor assembly not parallel to gyro input axes). The mechanical coupling mechanisms tend to pull the dither frequencies in orthogonal axes together, thereby creating real coning at dither frequency. Hence, even if single gyro dither frequencies are separate, the mechanical coupling can shift the frequencies toward each other, thereby creating correlated frequency components between axes, or coning. Another source of real high frequency coning is linear random vibrations into the strapdown system that produce correlated frequency rotary sensor assembly motion in orthogonal axes due to sensor assembly/elastomeric mount asymmetries.

The real coning motion effects described above would not be a problem in themselves, since laser gyros have the bandwidth and sensitivity required for accurate measurement of these effects. The problem arises from pseudo-coning created at dither frequency, also due to dither mechanical interaction. A classical example is sensor assembly bending induced by the dither reaction torque which produces false gyro outputs at dither frequency (e.g., due to bending in the mechanism used to measure and remove gyro block/case relative angular dither motion from the gyro output, or gyro mount twisting about the gyro input axis).

Exact and sophisticated mechanical design techniques must be used in the overall sensor, sensor assembly, and sensor assembly mount to assure that pseudo-coning effects are negligible below the frequencies where real coning exists and has to be measured (33, 34). The coning computation algorithm in the strapdown computer (33) can then be run at an iteration rate that is only high enough to measure the real coning motion frequency effects (i.e., so that high frequency pseudo-coning effects are attenuated). Classical techniques utilized to minimize pseudo-coning effects are to design for stiffness in the sensor assembly, design for mechanical symmetry in the sensor assembly to minimize mechanical dither cross-coupling between gyro axes, and to assure sufficient gyro dither frequency separation so that the tendency for frequency pulling together is minimized. If performed properly, a total design can be achieved that meets overall system requirements under external vibration. Proper design is more easily achieved for benign vibration environments (e.g., commercial aircraft).

## 5.2.2 Magnetic Mirror Bias

The magnetic-mirror concept is a nonmechanical biasing technique based on the transverse

magneto-optic Kerr effect (14, 18, 21). A special inner coating (e.g., ferromagnetic metal) is applied to one of the laser gyro mirrors which, when magnetized normal to the plane of incidence by an applied magnetic field, imparts a nonreciprocal (i.e., opposite) phase shift between the clockwise and counterclockwise laser beams. This produces an apparent differential path-length shift between the laser beams which generates a frequency difference or output rate. The result is a bias imposed on the gyro output that is controllable by the applied magnetic field. Bias uncertainties are compensated through use of alternating bias control (i.e., square-wave dithering of the applied magnetic field). The magnetic field intensity is set at a high enough level to operate the magnetic mirror in a saturated state. In this way, bias shifts generated by stray magnetic fields are minimized.

The advantage of the magnetic mirror is the elimination of the need for mechanical dither, its associated design complications, and size/weight penalties. A problem area for the magnetic mirror has been difficulties in generating a large enough bias for the 0.63 micron laser gyro due to low reflectance of the ferromagnetic coating (14, 20). The resulting loss must be compensated by higher gain in the laser helium-neon discharge. For the 0.63 micron laser, high gain cannot be tolerated because the laser begins to resonate unwanted mode shapes that deteriorate performance. The net result is that the magnetic mirror biasing capability must be diluted by appropriate layering of dielectric coatings on the mirror to recover reflectance. The net bias levels achieved with this approach have not been sufficient to adequately compensate lock-in. (It should be noted that ferromagnetic magnetic mirror technology has been successfully applied to the lesser accurate 1.15 micron laser gyro which can be operated at a higher gain before multimoding problems develop (24)). Another problem area for magnetic mirror technology has been the introduction of residual nonreciprocal phase shifts between the incident laser beams that are temperature sensitive. The result is a bias instability that is temperature sensitive and which produces turn-on transients.

Recent work on laser gyro magnetic mirror technology has concentrated on the development of a garnet magnetic mirror in which the dielectric layer coatings on the laser mirror are made with a transparent garnet film that produces nonreciprocal phase shift to incident light on application of a magnetic field (20). The result has been that the loss effect (associated with the ferromagnetic magnetic mirror technology) has been significantly reduced so that high bias levels can be achieved with 0.63 micron lasers. Current design work is concentrating on doping the garnet material to reduce the effect of residual nonreciprocal temperature sensitive phase shifts that have remained with the new garnet mirror technology. Engineering personnel associated with these developments are predicting a breakthrough within the next year based on experimental results achieved to date on doped garnet coatings.

### 5.2.3 Multioscillator Laser Gyro

Conventional two-beam (clockwise and counterclockwise) laser gyros are designed to amplify plane polarized laser light (i.e., in which the electric vector normal to the laser beam is either perpendicular to the lasing plane (S-polarization) or in the lasing plane (P-polarization)). Triangular lasers typically use the former polarization while square laser gyros typically use the latter. In the case of the multioscillator laser gyro (26, 27), circular polarization is used in which both S and P modes are simultaneously excited, but at one quarter wavelength phase shifted from one another. The result is a combined electric vector polarization that spirals between S and P, denoted as circular polarization. Right circularly polarized (RCP) or left circularly polarized (LCP) light is generated by creating a plus or minus quarter wavelength shift between the S and P waves, thereby creating a right or left sense spiralling electric vector wave.

In the multioscillator, both RCP and LCP laser beams are created in the same cavity, each with clockwise and counterclockwise components (i.e., a four-beam laser gyro). The two polarization states are excited by a reciprocal polarization rotator (e.g., a quartz crystal) in the beam path that imparts an additional spiral rotation to the circularly polarized light, and which operates identically on both the clockwise and counterclockwise components of the RCP or LCP beams (i.e., reciprocal). The additional rotation adds to the spiralling for the RCP beam and retards the spiraling of the LCP beam. The effect of the added rotation on the RCP beam is to resonate the light components with decreased wavelength such that a net spiral angle reduction is achieved around the beam path to match the spiral angle increase across the rotator. As a result, the RCP beam (both the clockwise and counterclockwise components) are up-shifted in frequency (proportional to the wavelength decrease). The opposite effect is created in the LCP light which is down-shifted in frequency by the same amount that the RCP light frequency is up-shifted. As for the two-beam laser gyro, each polarization state (RCP or LCP) contains a clockwise (CW) and a counterclockwise (CCW) beam component. Hence, two sets of CW and CCW beams are established, one RCP and the other LCP, each operating at a different center frequency. Each set is used to generate an independent output signal equal to the frequency difference between the CW and CCW beams. As for the two-beam laser gyro, the frequency difference output from each polarization state is proportional to input rotation rate. Also, as for the two-beam laser gyro, the frequency difference output from the RCP and LCP lasers experience lock-in which pull the CW and CCW frequencies together at low input rates.

In order to overcome lock-in, a nonreciprocal polarization rotator is introduced into the beam path which rotates circularly polarized light in the opposite sense for clockwise

compared to counterclockwise beams. Hence, a frequency shift is imparted between the clockwise and counterclockwise beams (i.e., a bias) for both the RCP and LCP light. The frequency difference is maintained at a high enough level to remain far from the lock-in region under frequency shifts produced by angular rate inputs. The common means for introducing the nonreciprocal bias in the multioscillator laser gyro has been through use of a Faraday rotator consisting of a piece of amorphous glass placed in the beam path with a magnetic field applied across it parallel to the beam. The resulting Faraday effect introduces the desired frequency bias on the circularly polarized light that is in the opposite sense for the LCP compared to the RCP light beams. As a result, the RCP beam output (i.e., the difference between the clockwise and counterclockwise RCP beam frequencies) is positively biased, while the LCP beam frequency difference output is negatively biased by an equal amount.

By summing the outputs from the RCP and LCP beam sets, the input rate sensitivity is doubled, while the Faraday bias effect is cancelled. The cancelling of the bias by summing both outputs eliminates the need for alternating bias to compensate for Faraday rotator gain uncertainties. Elimination of the oscillating bias eliminates a main source of laser gyro random noise (i.e., dithering through the lock-in region). Hence, the random noise in the multioscillator is lower, and closer to the theoretical limit created by random gain and loss of photons from the laser beams (25, 26).

**5.2.3.1 Principal Error Sources** - The basic principal behind lock-in compensation in the multioscillator laser gyro relies on the Faraday bias (and Faraday bias uncertainties) being equal between the two laser beam sets so that they cancel one another. In practice, this is not totally true, to a large degree because the operating frequencies of the left and right circularly polarized laser sets are different by design. This frequency difference causes each to behave slightly differently to the Faraday bias, producing a net residual error when combined. The error is both temperature and magnetically sensitive, requiring some degree of magnetic shielding and temperature measurement compensation.

Another source of bias error in the multioscillator is variations in the lock-in characteristic between the right and left circularly polarized beams. Even through the Faraday bias keeps the lasers well outside of the lock-in region, small scale factor nonlinearities still exist at the bias point caused by lock-in. Because the lock-in rates for the two beam sets differ, when the gyro outputs are summed, the residual lock-in error effects at the bias point do not cancel. The resulting bias error created is temperature sensitive and can have unpredictable variations over time.

Multioscillator design groups claim that the above effects are for the most part, predictable and can be compensated sufficiently for satisfactory operation in high accuracy applications.

Two areas where serious errors can develop and are not easily compensated arise from anisotropic and birefringence effects introduced in the light beams as they pass through a quartz crystal reciprocal polarization rotator and Faraday nonreciprocal rotator. The net effect is to introduce unpredictable nonreciprocal path length variation between all four beams which are temperature, acceleration and magnetically sensitive.

Recent advances in multioscillator design techniques have replaced the quartz crystal reciprocal polarization rotator with an out-of-plane beam path geometry that rotates the laser beam by optical reflection at the mirrors (thereby, mimicking the rotational effect of the quartz crystal) (27). The result is elimination of birefringence effects originally created by the presence of the quartz crystal in the beam path. Current work on the multioscillator is addressing improved methods for providing nonreciprocal polarization rotation that have small and more predictable error characteristics than were achieved with original Faraday rotator design configurations.

### 5.3 Laser Gyro Performance And Application Areas

Over the past 6 years, the ring laser gyro (RLG) has progressed from advanced development into full scale production in 1-nmph strapdown inertial navigation applications. The successful 1-nmph laser gyro system programs to date have utilized the 0.63 micron transition with mechanical dither. Systems in the 1-nmph range have been developed by several competing manufacturing groups for both commercial and military application.

Performance advances in RLG technology have been rapid. Continuing advances in laser gyro mirror technology has reduced lock-in (and random noise) by more than an order of magnitude over the past eight years. Lock-in rates lower than 0.0003 deg/hr have been reported. Advanced development programs are now in progress to design laser gyros with performance capabilities required for 0.1 nmph navigation applications.

Principal problems remaining with RLG technology are size and weight for the high performance applications, and size, weight, and cost for the lower accuracy applications. For the higher performance applications, the total weight of an RLG strapdown inertial navigation system is typically 30% higher than its comparable gimbaled system counterpart. Significant cost, reliability, and reaction time benefits for the RLG system, however, make

it an attractive alternative to the traditional gimbaled system. It is generally conceded that laser gyro performance in the lower accuracy AHRS and tactical missile midcourse guidance application areas is superior to the competing strapdown RIG or TRG strapdown technologies, however, size, weight, and cost advantages for the RIG or TRG with acceptable performance are prevailing factors today that continue to restrict entry of the RLG into the lower performance application areas.

Performance advances in future RLG's may make it possible to build smaller, lighter weight laser gyro systems for the lower performance market. Advances in nonmechanically dithered RLG technology may make it possible in the future to build a small size cost/performance competitive integrated 3-axis laser gyro sensor assembly (1, 24) in a single Zerodur structure using interleaved laser paths to reduce net size/weight. If advances in mirror technology continue to reduce lock-in rates and associated dither amplitude requirements, mechanically dithered RLG system size/weight will also be reduced in the future. Production learning is expected to be the determining factor that will decide the degree to which laser gyro production costs will be reduced in the future to be competitive with the lower performance RIG and TRG strapdown sensors. For the higher performance strapdown applications areas, strapdown RIG and TRG manufacturer's generally concede that the ring laser gyro is now the industry standard, and not a viable competition area for higher performance but more expensive versions of strapdown TRG or RIG technology.

#### 6. FIBER-OPTIC ROTATION RATE SENSOR

One of the newer rate sensor technologies that has emerged over the past few years is the fiber-optic rotation rate sensor (28). The concept for the device is illustrated in Figure 8. Light generated from a suitable light source at a specified design frequency is transmitted through a fiber-optic coil. The light beam is first split by a beam-splitter so that half the radiation traverses the coil in the clockwise (CW) direction, and half in the counterclockwise (CCW) direction. The emerging light from both ends of the coil are then recombined at the beam splitter, and transmitted onto a photodetector. The photodetector output power is proportional to the average intensity of the recombined light.

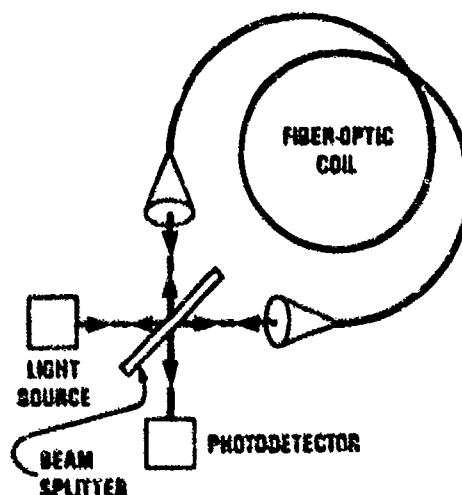


Figure 8 - Basic fiber-optic rotation rate sensor concept

Under rotation of the device about an axis normal to the plane of the fiber-optic coil, the effective optical path length is changed for the CW compared to the CCW beams in a manner similar to the ring laser gyro. In the direction of rotation, the path length increases (i.e., a photon of light has to traverse the length of the coil plus the distance that the coil has been rotated during the traversal period). In the direction opposite to the rotation, the light traverses the length of the coil, minus the distance that the coil has been rotated during the traversal period. The difference between the CCW and CW optical path lengths, then, is twice the distance of rotation, or:

$$\Delta L = 2 \frac{L}{c} \frac{D}{2} \omega = \frac{L D \omega}{c}$$

where

L = Total fiber length

- D = Diameter of coil (assumed circular)  
 $\Delta L$  = Difference between CW and CCW optical path-lengths  
 $\omega$  = Input angular rate  
 C = Speed of light

This corresponds to a phase shift between the CW and CCW light beams emerging from the coil given by :

$$\Delta\phi = 2\pi \frac{\Delta L}{\lambda} = 2\pi \frac{L D}{C \lambda} \omega \quad (3)$$

where

- $\lambda$  = Wavelength of light source

Thus, the phase angle between the emerging light beams becomes proportional to the input angular rate. This contrasts with the ring laser gyro resonator for which the phase angle change is proportional to the integral of the input rate (see Equation (1)). Hence, the fiber-optic rotation sensor is a "rate gyro" while the laser gyro is a "rate integrating gyro". The other difference between the two sensors is that the laser gyro CW and CCW beam frequencies are shifted from each other proportional to the input rotation rate (due to the self-resonance of the laser); the frequencies for the CW and CCW beams in the fiber-optic rate sensor remain equal under rotation rates.

The photodetector in Figure 8 is used to sense the phase shift between the CW and CCW beams. The amplitude of the combined beams at the photodiode equals the sum of the individual beam amplitudes, including the phase shift factor. The result is a combined beam intensity which is maximum for  $\Delta\phi = 0$  and minimum (zero) for  $\Delta\phi = \pi$  (i.e., varies as  $\cos^2(\Delta\phi/2)$ ). The photodetector output is proportional to the light intensity, hence, also varies approximately as  $\cos^2(\Delta\phi/2)$ .

In order to achieve high sensitivity (high scale factor), the length L of the fiber coil is large. A typical value of L = 400 meters with D = 0.1 meters and  $\lambda = 0.82$  microns produces a  $\Delta\phi$  from equation (3) of approximately one radian at 1 rad/sec input rate.

#### 6.1 Practical Design Refinements

As depicted in Figure 8, the fiber-optic rotation rate sensor has fundamental error mechanisms that make it impractical to implement. Among these are large scale factor errors associated with photodetector scale factor uncertainties, light source intensity variations, and light amplitude losses in the fiber; loss of rate sensitivity around zero input rate (due to the  $\cos^2(\Delta\phi/2)$  output characteristic of the photodetector; phase angle variations due to mechanical movement between the beam splitter and fiber that produce changes in path length between the CW and CCW beams; and polarization state differences between the CW and CCW beams that produce phase shifts due to nonreciprocal birefringence and anisotropic effects in the fiber material that are aggravated by environmental exposure. To overcome these fundamental problems, recent fiber-optic rotation sensor configurations (28) have adopted refined interface and control elements such as those depicted in Figure 9.

In Figure 9, the discrete component beam-splitter in Figure 8 is replaced by fiber-optic couplers which consist of integrated fiber-optic junctions that split entering beams 50% to the left and 50% to the right. A polarizer (28) is included to suppress unwanted polarization states in the light. The fiber itself is specifically manufactured to preserve a single polarization state (28) ("polarization preserving fiber"). In this manner, nonreciprocal fiber-beam interactions are suppressed.

A light source (typically a super-luminescent diode such as Gallium Arsenide) transmits narrow frequency bandwidth light\* into the fiber that splits into CW and CCW components at the coupler junction. Acousto-optic shifters (A/O) (such as Bragg cells\*\*) at the end of

\*Note - Original fiber-optic sensors used laser light. One of the major technological break-throughs for the fiber-optic sensor was replacement of the coherent laser light with a broader spectrum source. The result was a significant reduction in nonreciprocal beam/fiber interaction error mechanisms due to the shorter correlation distance for the broader spectrum light (28, 29).

\*\*Note - A Bragg cell (28) is typically mechanized as a piezoelectric device that imparts an acoustical vibration transverse to the light beam at its input drive frequency. The result is a bending of the light (by the "Bragg angle") with an accompanying frequency shift in the light passing through the cell equal to the Bragg cell drive frequency.

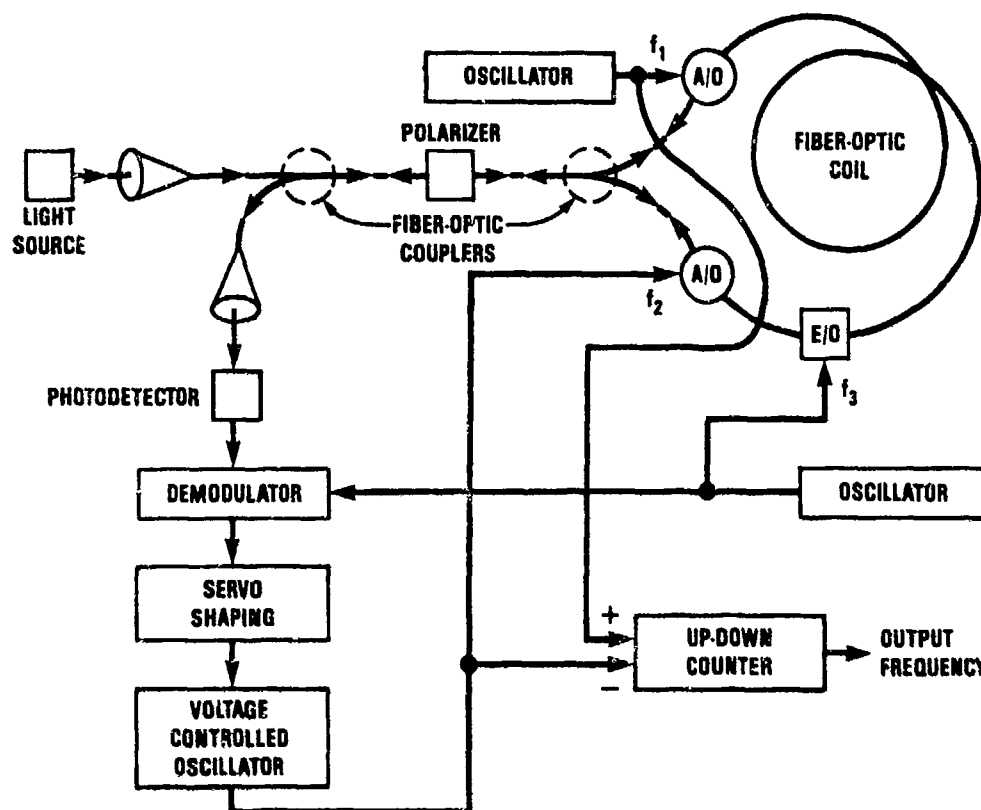


Figure 9 - Improved fiber-optic rotation rate sensor configuration.

the fiber coil are then used to generate a controlled phase shift in the light illuminating the photodetector.

To function properly, each Bragg cell in Figure 9 must be biased at a large offset frequency  $F_1$  (typically 20 MHz). A Bragg cell mounted at one end of the coil is driven directly at the bias frequency  $F_1$  (see Figure 9) which up-shifts the light leaving the cell by  $F_1$  from the light entering the cell. The light entering from the left (the clockwise CW beam in Figure 9) must traverse the length of the coil at the up-shifted frequency before it leaves the coil and illuminates the photodetector. The beam entering from the right (the counterclockwise CCW beam in Figure 9), on the other hand, immediately leaves the coil and illuminates the detector after it is frequency up-shifted. The net result is that the CW beam travels a further distance at the up-shifted frequency than the CCW beam, thereby generating a net phase shift between the CW and CCW beams at the photodetector proportional to  $F_1$  and the coil length.

The Bragg cell at the opposite end of the coil is driven at  $F_2$  which generates a phase shift at the photodiode in the opposite sense to that created by the  $F_1$  Bragg cell. The  $F_2$  frequency is controlled in servo fashion to maintain the photodetector output at peak power (i.e., zero net phase angle). Under zero input angular rate, the  $F_2$  servo drives  $F_2$  to equal  $F_1$  (i.e., so that equal and opposite phase shifts are created that cancel one-another). Under input angular rate, the servo creates a frequency difference between  $F_2$  and  $F_1$ , the device output in Figure 9, proportional to the input angular rate (that generates an equivalent phase shift at the readout to null the phase shift created by input rotation). It is easily demonstrated that the frequency difference generated to achieve a net zero phase angle is given by:

$$F_2 - F_1 = \frac{4A}{\lambda L} \omega$$

(5)

where

$l$  = Length around one coil of the fiber (which typically consists of several coils).

If equation (5) is compared with equation (1) for the laser gyro resonator, it should be clear that they are identical on an integral basis (i.e., the frequency difference pulse count cycles from equation (5) times  $2\pi$  radians/cycle is proportional to the input angle by the same factor that, in equation (1), relates RLG output fringe angle change to input angle change.

Figure 9 also includes an electro-optic phase shifter (E/O) driven at frequency  $F_3$  at one end of the fiber, which imparts an oscillating path length change to the CW and CCW beams passing through (Note: The E/O is typically mechanized as a piezoelectric actuated "stretcher" which physically changes the length of the fiber by introducing stresses in the fiber proportional to applied voltage (28, 29). This induces an equivalent phase shift in the light). Because the E/O driver is at one end of the coil, the light beam passing out of the coil delivers the phase shift effect first to the photodetector. The beam traveling in the opposite direction has to traverse a longer length of fiber to the photodetector, hence, delivers its phase shift, by an equal amount, later. The delay creates an alternating phase bias at the photodiode mixed beam output, generating an oscillation of the output about the peak power point. By comparing the positive half cycle output decrease with the negative cycle decrease, a linear signal can be generated proportional to the average deviation of the input light phase angle difference from zero. The linear signal is generated in the phase sensitive demodulator shown in Figure 9 driven by  $F_3$ . The result is a signal out of the demodulator that is linearly proportional to the  $\Delta\phi$  phase deviation from zero, thereby eliminating the  $\cos^2(\Delta\phi/2)$  sensitivity problem around  $\Delta\phi = 0$  that exists without the E/O device.

The basic advantages for the Figure 9 compared to the Figure 8 mechanization approach are the elimination of the discrete light/beam-splitter/fiber junctions, thereby reducing phase shift errors caused by mechanical movement; elimination of the photodetector zero-phase angle sensitivity problem through use of the E/O demodulator; and, through the closed-loop servo operation that maintains the phase angle signal at null, elimination of scale factor errors associated with light source intensity, optical intensity losses in the fiber and beam-splitters, and photodetector scale factor uncertainties.

## 6.2 Development Status And Application Areas

The basic motivation behind the development of the fiber-optic rate sensor was to design a low cost alternative to the ring laser gyro that was inherently void of lock-in problems. The resonant characteristic of the laser gyro which regenerates its light source by stimulated emission, is the transfer mechanism that couples the CW and CCW beams together from back-scatter, producing lock-in. For the fiber-optic rate sensor, the light source is external to the sensing ring, hence, does not amplify the effects of back-scatter. As a result, the lock-in phenomenon associated with the laser gyro is absent in the fiber-optic sensor. This has been proven experimentally (29). The rationale behind the projected low cost of the fiber-optic sensor is that use of fiber-optics and integrated-optics technologies should reduce labor hours associated with device manufacture. It also assumes continuing reductions in the cost of high quality optical fiber which has been occurring over the past few years. From a performance standpoint, the fiber-optic rotation sensor is not expected to compete with the high performance laser gyro for accuracy, but is envisioned as a competitor to the lower cost autopilot, and eventually tactical missile and AHRS quality gyros.

Much has been accomplished since 1976 when the fiber-optic rotation sensor concept was originally conceived. To a large degree, these accomplishments are summarized by the evolution of the concept from its original form (in Figure 8) to its more refined practical form (in Figure 9). Nevertheless, much remains to be accomplished before this device can be considered a serious competitor with mature low cost conventional spinning wheel gyro technology or new lower cost/medium performance laser gyro technology. The device has still to be designed into a practical form that is producible at low cost, and which achieves overall performance goals over operational environments in a reasonable form factor. To a large extent the development status reflects the level of funding commitment assigned by individual groups toward device development. Although many small funded activities have existed over the past 8 years, few dedicated programs have been heavily funded. From another standpoint, the funding limits could reflect lack of confidence by funding agencies in the new technology, or a lack of available funds to pursue new technologies after completing heavy investments in recent technologies that are only now entering large scale production (e.g., the laser gyro).

Some of the technical problems that remain for the fiber-optic rotation rate sensor (28) include larger than desired size (2 to 4 inches in diameter) for the fiber-optic ring to avoid introducing beam interactions with the fiber walls under tight fiber turns; scale factor errors due to photodiode output frequency variations with temperature; bias errors associated with photodiode output frequency side-bands creating phase offsets at the photodetector; bias errors created from large required Bragg cell drive frequency offsets coupled with variations in the CW and CCW Bragg biased coil lengths due to off-nominal

variations between the Bragg cell distances to the fiber-optic coupler (see Figure 9); bias errors associated with the E/O demodulator electronics loop; bandwidth limits associated with the closed-loop operation in Figure 9; and increasing complexity of the sensor configuration to resolve problem areas. Virtually no data has been published on the performance of the fiber-optic rate sensor under dynamic environments. One of the principal potential error mechanisms for the device (as for all angular rate sensing instruments) is bias error created under dynamic temperature, mechanical vibration, acoustic vibration, acceleration, and magnetic environments. Fiber-optic rate sensor enthusiasts remain confident that these problems can be resolved, given time and funding. For evidence they point to the significant performance advances made over the past eight years, where the fiber-optic rate sensor has progressed from an original concept that could barely detect earth's rate, to current technology versions that have demonstrated milli-earth-rate sensitivities (29).

## 7. PENDULOUS ACCELEROMETER

The pendulous accelerometer (Figure 10) (1) consists of a hinged pendulum assembly, a moving-coil signal-generator/pickoff that senses angular movement of the pendulum from a nominally null position, and a permanent-magnet torque-generator that enables the pendulum to be torqued by electrical input. The torquer magnet is fixed to the accelerometer case, and the coil assembly is mounted to the pendulum. Delicate flex leads provide electrical access to the coil across the pendulum/case hinge junction. Electronics are included for pickoff readout and for generating current to the torquer.

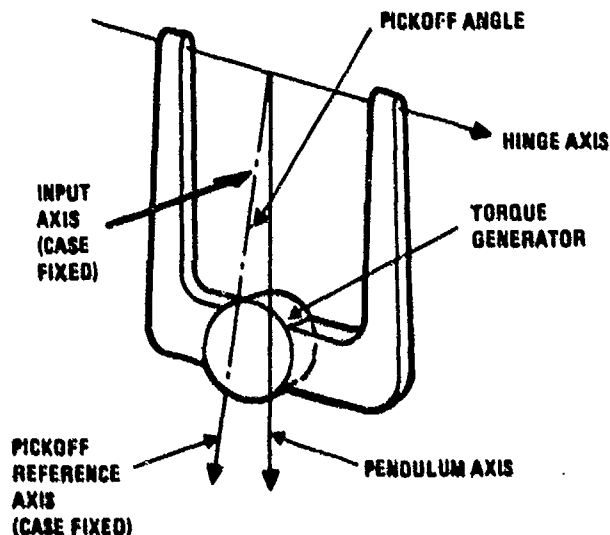


Figure 10 - Electrically servoed pendulous accelerometer concept.

The device is operated in the captured mode by applying electrical current to the torquer at the proper magnitude and phasing to maintain the pickoff at null. Under these conditions, the electrically generated torque on the pendulum balances the dynamic torque generated by input acceleration normal to the pendulum plane. Hence, the electrical current through the torquer becomes proportional to input acceleration, and is the output signal for the device.

Mechanization approaches for the pendulous accelerometer (1) vary between manufacturers and generally fall into two categories: fluid filled and dry units. Fluid-filled devices use a viscous fluid in the cavity between the pendulum and case for damping and partial compensation. The dry units use dry air, nitrogen, or electromagnetic damping.

The hinge element for the pendulous accelerometer is a flexible member that is stiff normal to the hinge line to maintain mechanical stability of the hinge axis relative to the case under dynamic loading, but flexible about the hinge line to minimize unpredictable spring restraint torques that cannot be distinguished from acceleration inputs. Materials selected for the hinge are chosen for low mechanical hysteresis to minimize unpredictable spring-torque errors. To minimize hysteresis effects, the hinge dimensions are selected to assure that hinge stresses under dynamic inputs and pendulum movement are well below the yield-stress for the hinge material. Beryllium-copper has been a commonly used pendulum-hinge material due to its high ratio of yield-stress to Young's modulus (i.e., the ability to provide large flexures without exceeding material yield-stress). Another successful

design approach for dry accelerometers has utilized fused quartz for both the hinge and pendulum by etching the complete assembly from a single-piece quartz substrate (1).

### 7.1 Performance And Application Areas

The pendulous accelerometer continues to be the primary mechanization approach being used for almost all strapdown applications. Design refinements over the past 6 years now provide units from several manufacturers that meet 1.0 nmph strapdown inertial navigation requirements in heaterless configurations. The heaterless configuration operates without temperature controls and achieves its accuracy through thermal modeling of the sensor errors in the strapdown system computer based on temperature measurements taken with temperature probes mounted within the sensing unit. The heaterless accelerometer configuration has been perfected within recent years for operation with ring laser gyros which are also operated heaterless using direct path-length control to stabilize performance (Note: Use of heaters to control temperature and stabilize performance with the ring laser gyro is impractical due to the long thermal time constant of the Zerodur material from which it is constructed, and the associated reaction time penalty that would be introduced from turn-on until temperature/performance stabilization. Laser gyro performance variations with temperature are also compensated by thermal modeling). It is highly fortunate that pendulous accelerometer designs originally developed for heated operation (to stabilize performance), have been predictable enough thermally, to allow accurate characterization over their complete temperature range by analytical modeling using temperature measurements. Hence, major design refinements for heaterless operation have not been necessary.

Most accelerometers today are of the dry pendulous metal flexure hinge variety (1). Design refinements in quartz hinge design configurations (1) (most notably in the plating technology used to conduct current across the hinge into the pendulum-mounted torquer coil to minimize hysteresis) have provided a rugged unit that meets 1.0 nmph strapdown inertial navigation accuracy requirements.

Experimental pendulous accelerometers have recently provided indications that identifiable further design refinements will make it possible to achieve the accuracy improvements needed for the advanced 0.1 nmph INS applications. Advanced engineering development programs are currently being funded (at a fairly modest level) to develop and evaluate these performance improvements.

Unit costs for the pendulous accelerometer, although acceptable, still remain higher than desirable, particularly in the higher accuracy applications. Competitive sourcing in some applications has created the environment needed to reduce costs to some extent through design, manufacturing, and test improvements. Increased production volume has added to cost reduction through learning and improved tooling/automation techniques. However, the production volume has not been sufficient to develop the automatic manufacturing technologies needed to make major in-roads in cost reduction. Nevertheless, the pendulous accelerometer cost is acceptable for most applications, compared to the cost of other strapdown system elements.

## 8. TORQUE-LOOP MECHANIZATION APPROACHES FOR TORQUE REBALANCE INSTRUMENTS

The implementation of the torque loop for the torque-to-balance instruments (e.g., floated rate-integrating gyro, tuned-rotor gyro, pendulous accelerometer) continue to be mechanized using different approaches, depending on manufacturer: digital pulse-rebalance or analog-rebalance with follow-up pulse-rebalance logic, using pulse-on-demand or pulse-width-modulated forced limit-cycle techniques (1). Little data has been published on the performance of these electrical circuits, an unfortunate circumstance, particularly since their accuracy is a key contributor to the overall performance of the instrument they are designed to operate with. Performance data advertized as representative of particular sensors does not always include the effect of the digital pulse-rebalance circuitry (i.e., the data was taken on an analog basis at the basic instrument level). This becomes of greater concern when one considers the more demanding application areas that can require dynamic ranges (maximum input versus bias accuracy) in the  $10^6$  to  $10^7$  category.

## 9. THE VIBRATING BEAM ACCELEROMETER

Much of the cost for conventional pendulous electrically-servoed accelerometers is associated with the torque-generator and electronics needed to close-the-loop on the instrument and generate precision pulse outputs representing quantized increments of integrated input acceleration (1). The vibrating beam accelerometer replaces the torque-rebalance mechanism with an open-loop direct-digital-output transducer based on quartz-crystal oscillator technology (30, 31, 32). The concept is depicted in Figure 11.

In Figure 11, two quartz-crystal beams are mounted symmetrically back-to-back so that each axially supports a proof mass pendulum. Each beam is vibrated at its resonant frequency by an electronics loop in a manner similar to the method used to sustain amplitude in quartz-crystal oscillator clock references. In the absence of acceleration along the

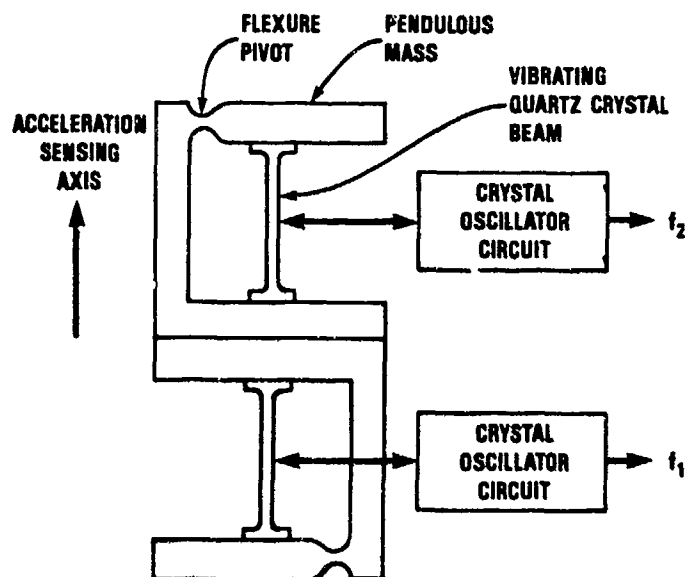


Figure 11 - Vibrating beam accelerometer concept.

acceleration sensing axis, both beams are selected to nominally resonate at the same frequency. Under applied acceleration, one beam is placed in compression and the other in tension by the inertial reaction of the pendulous proof masses. This produces an increase in frequency for the beam in tension, and a decrease in frequency for the beam in compression. The frequency difference ( $f_2 - f_1$  in Figure (11)) is a direct digital output proportional to the input acceleration.

The symmetrical arrangement of the beams produces a cancellation of several error effects that would exist for one beam mounted individually. Error effects that are nominally cancelled include nominal beam frequency variations with temperature and aging, asymmetrical scale factor nonlinearities, anisoinertia errors (1), and vibropendulous errors (1) that are common between the individual beam assemblies.

#### 9.1 Design Considerations And Application Areas

The vibrating beam accelerometer is being designed as a lower cost alternative to the conventional pendulous electrically-servoed accelerometer for strapdown applications. Cost reductions are expected to be achieved through elimination of the complex electro-mechanical assembly associated with the pendulous accelerometer torque-generator, and elimination of complex torque-to-balance and pulse quantizer readout electronics.

The ultimate success of the vibrating beam accelerometer will depend on whether its accuracy capabilities will approach those of mature technology pendulous accelerometers at a competitive price. Error mechanisms in the vibrating beam accelerometer arise from unpredictable variations between the two beam assemblies that are temperature, vibration sensitive and which vary over time. One of the more important error mechanisms that must be dealt with in the design of the unit is the potential problem of mechanical coupling between the beam assemblies that pull the frequencies together under low input acceleration (an effect similar to lock-in for laser gyros). The result is a detection threshold for the unit that is a function of the strength of the mechanical coupling. The key to the design of an accurate vibrating beam accelerometer lies in the ability to isolate one crystal beam from the other. One approach being used to achieve isolation is through application of a dual-beam construction (32) for each of the crystal beam assemblies as illustrated in Figure 12.

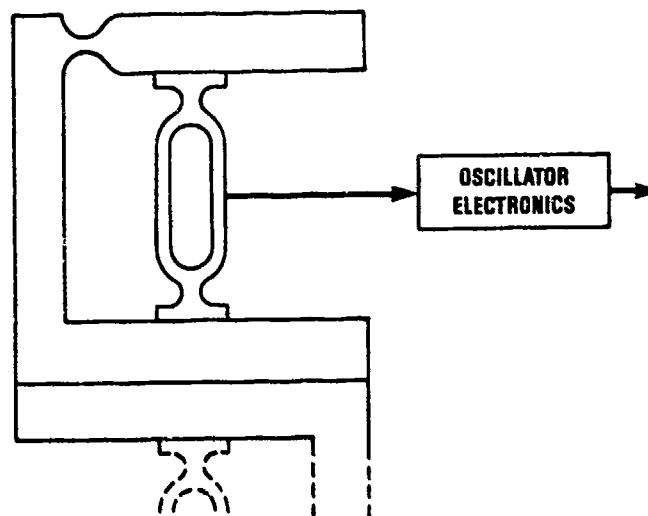


Figure 12 - Dual-beam crystal oscillator concept.

In Figure 12, each beam assembly is composed of an integral dual-beam arrangement in which the beam elements vibrate in opposition (180 degrees out of phase). The resulting counter-vibration allows each beam movement to be counter-acted mechanically by the other such that no net vibration is transmitted into the mount (i.e., similar to a tuning fork). The result is that mechanical coupling mechanisms between the independent dual-beam assemblies are minimized.

A problem area being addressed in the design of the vibrating beam accelerometer is the output resolution. Typical mechanizations are based on using crystals with a 40 KHz center frequency (zero input acceleration) with 10% variation over the design acceleration range. Hence, the inherent maximum frequency output of the device (beam frequency difference) under maximum input acceleration is typically 5 to 10 KHz. For the higher accuracy applications, this resolution is generally too coarse (by at least an order of magnitude under certain conditions). In order to enhance the basic resolution, design techniques being investigated include using time measurement between frequency difference pulses as the output, or use of digital phase-lock loop external circuitry to generate higher frequency waveforms whose integral tracks the frequency difference output signal.

The vibrating beam accelerometer is still in its development stage with units becoming available for evaluation by test groups this year. Developmental test results reported to date have been encouraging. It is too early at this time to predict what the ultimate cost/performance of the device will be compared to mature pendulous accelerometer technology.

#### 10. CONCLUDING REMARKS

Over the past six years, the laser gyro has emerged as the rate sensor most suitable for the high performance strapdown applications. Floated rate-integrating and tuned-rotor gyro technologies continue to be the most suitable rate sensors for the low-to-medium performance/low-cost application areas where small size is also important. It is expected that cost and size reductions for the laser gyro will broaden its applicability range in the future so that it will eventually dominate the medium accuracy performance areas as well. It is too early to predict whether the laser gyro will ever be of a low enough cost to successfully compete in the lower accuracy tactical missile application areas.

Pendulous accelerometer technology continues to be the main stay for strapdown applications. Performance advances and some cost reductions over the past few years have enabled this instrument to remain compatible with overall strapdown system cost/performance goals. To generate a significant cost reduction for strapdown accelerometers, the vibrating beam accelerometer is receiving attention by some development groups. Time will tell whether the cost/performance of this instrument will successfully compete with pendulous accelerometers in the future.

## 11. ACKNOWLEDGEMENTS

I would like to express my appreciation to engineering personnel in the following organizations who participated in valuable technical discussions on strapdown sensor technology during the preparation of this paper. These discussions provided the primary source of technical information for the paper.

Honeywell Avionics Division, Minneapolis, MN  
 Litton Guidance & Control Systems, Woodland Hills, CA  
 Naval Research Laboratory, Washington, DC  
 Raytheon Equipment Development Laboratories, Sudbury, MA  
 Rockwell Autonetics, Anaheim, CA  
 Singer Kearfott, Wayne, NJ  
 Sperry Gyroscope, Great Neck, NY  
 Sundstrand Data Control, Redmond, WA  
 Sundstrand Optical Technologies, Newbury Park, CA

## REFERENCES

1. Savage, Paul G., "Strapdown Sensors", "AGARD Lecture Series No. 95: Strapdown Inertial Systems - Theory And Applications", June 1978.
2. Savage, Paul G., "Laser Gyros In Strapdown Inertial Navigation Systems", IEEE PLANS, Hilton Inn, San Diego, CA, November 1 - 3, 1976
3. Dynamic Errors in Strapdown Inertial Navigation Systems, NASA Report CR-1962, December 1971.
4. Wrigley, W., Hollister, W.M., and Denhard, W.G., "Gyroscopic Theory, Design, and Instrumentation", M.I.T. Press, 1969.
5. Macomber, George R., and Fernandes, Manuel, Inertial Guidance Engineering, Prentice-Hall, Englewood Cliffs, New Jersey, 1962.
6. Howe, Edwin W., "A Free Rotor Gyro", Symposium on Unconventional Inertial Sensors, Farmingdale, New York, 1963.
7. Savet, Paul H., "New Trends in Non-floated Precision Gyroscopes", Grumman Research Department Memorandum RM-247J, October 1964.
8. Craig, Robert J.G., "Theory of Operation of Elastically Supported Tuned Gyroscope", IEEE Transactions on Aerospace and Electronic Systems, Vol. AES-8, No. 3, May 1972.
9. Craig, Robert J.G., "Theory of Errors of a Multigimbal, Elastically Supported, Tuned Gyroscope", IEEE Transactions on Aerospace and Electronic Systems, Vol. AES-8, No. 3, May 1972.
10. Craig, Robert J.G., "Dynamically Tuned Gyros in Strapdown Systems", AGARD Conference Proceedings No. 116 on Inertial Navigation Components and Systems, AD-758 127, Paris, France, February 1973.
11. Killpatrick, Joseph, "The Laser Gyro", IEEE Spectrum, October 1967.
12. Aronowitz, Frederick, "The Laser Gyro", Laser Applications, Vol. 1, Academic Press, New York, 1971.
13. Aronowitz, Frederick, and Collins R.J., "Mode Coupling Due to Back Scattering in a HeNe Traveling Wave Ring Laser", Applied Physics Letters, Vol. 9, No. 1, 1 July 1966.
14. Dewar, Dr. D., "The Laser Gyroscope", Royal Aeronautical Society, London, 12 January 1977.
15. Hanmons, Seridan W., and Ashby, Val J., "Mechanically Dithered RLG At The Quantum Limit", 0547-3578/82/0000-0388 Copyright 1982 IEEE.
16. Hutchings, T.J., and Stjern, D.C., "Scale Factor Non-Linearity of a Body Dithered Laser gyro", IEEE NAECON, 1978, Vol. 2, Pg. 549.
17. Hutchings, T., "Development And Test of A Small Body Dithered Laser Gyro", Electro-Optics/Laser 77 Conference & Exposition, Anaheim, CA, Oct. 25-27, 1977.
18. Henery, R.D., Whitcomb, E.C., and Vesical, V., "Ferrimagnetic Garnets As Laser Gyro Faraday Elements", Electro-Optics/Laser 77 Conference & Exposition, Anaheim, CA, Oct. 25-27, 1977.
19. Mark, John G., Ebner, Robert E., and Brown, Alison K., "Design of RLG Inertial Systems For High Vibration", IEEE PLANS, Atlantic City, NJ, December 6-9, 1982.

20. McClure, R.E., and Vaher E., "An Improved Ring Laser Bias Element", CH1336-7/78/0000-0544 Copyright 1978 IEEE.
21. McClure, R.E., "An Electrical Equivalent Circuit For The Transverse Magneto-Optic Effect In Thin Magnetic Films", International Magnetism Conference, Boston, MA, April 24, 1980.
22. Freiser, M.J., "A Survey of Magneto-Optics Effects", IEEE Transactions on Magnetism MAG-4, 152, 1968.
23. Dillon, Jr., J.F., "Magneto-Optical Properties of Magnetic Garnets", Physics of Magnetic Garnets, pp 379-415, A. Paoletti, ed; North Holland, 1978.
24. Morrison, R.F., Levinson, Dr. E., and Bryant Jr., B.L., "The SLIC-7 Laser Gyro, Inertial Guidance System", NAECON, Dayton, Ohio, 1977.
25. Dorshner, Terry A., Hermann, A. Haus, Holz, Michael, Smith, Irl W., and Statz, Hermann, "Laser Gyro At Quantum Limit", IEEE Journal of Quantum Electronics, Vol QE-16, No. 12, December 1980.
26. Mathews, James B., Gneses, Morris I., and Berg, Dennis S., "A High Resolution Laser Gyro", NAECON May 16-18, 1978, Dayton, Ohio.
27. Statz, H., Dorshner, Terry A., Holz, M., and Smith, Irl W., The Multioscillator Ring Laser Gyroscope, Raytheon Research Division Technical Report T-1096, January, 1983.
28. Ezekiel, S., and Arditty, H.J., ed. Fiber-Optic Rotation Sensors, Proceedings of the First International Conference, M.I.T., Cambridge, MA, November 9-11, 1982; Published in Springer Series in Optical Sciences, Vol. 32, Schawlow, Arthur L., ed., Springer-Verlag Berlin Heidelberg New York 1982.
29. Burns, W.K., Moeller, R.P., Villarruel, C.A., and Abebe, M., "Fiber-Optic Gyroscope with Polarization-Holding Fiber", Optics Letters, Vol. 8, No. 10, October 1983.
30. Albert, William C., and Weber Raymond E., "Vibrating Beam Accelerometer For Strapdown Applications", IEEE PLANS, Atlantic City, NJ, December 6-9, 1982.
31. Albert, William C., "Vibrating Quartz Crystal Beam Accelerometer", Copyright ISA, 1982, ISBN: 0-87664-689-5.
32. Gogic, A.M., and Peters, R.B., "Description And Test Methods For A Frequency Output Accelerometer", Inertial Navigation Test Symposium, Holloman AFB, 1983.
33. Savage, P.G., "Strapdown System Algorithms". AJARD Lecture Series No. 133: Advances In Strapdown Inertial Systems, May 1984.
34. Savage, P.G., Introduction To Strapdown Inertial Systems, June 1, 1983 (Third Printing), and Introduction To Strapdown Inertial Navigation Systems - Supplemental Material, November 14, 1983; Third Strapdown Associates Open Seminar On Strapdown Inertial Navigation Systems, Marquette Inn, Minneapolis, MN, Nov. 14-18, 1983.